Near-field imaging with two transmission gratings for submicrometer localization of atoms

O. Carnal,* Q. A. Turchette,† and H. J. Kimble
California Institute of Technology, Norman Bridge Laboratory of Physics 12-33, Pasadena, California 91125
(Received 21 April 1994)

We show theoretically that an atomic pattern with period d can be obtained with 100% visibility even for an infinitely extended source by sending atoms through two transmission gratings with periods d and $d/2$, respectively, and separated by half the Talbot length $L_T/2=d^2/2\lambda_{dB}$, where λ_{dB} is the atomic wavelength and the source is infinitely far away. For a finite source distance, as would be attainable in any real experiment, a small correction to the grating periods and separations restores the period-d pattern. This effect is closely related to the Talbot and Lau effects in classical optics and can be used to localize atoms to a submicrometer scale without a compromise in atomic flux. We first derive compact analytical formulas for the idealized case of a monochromatic source and large gratings and then verify numerically that a finite grating size and velocity dispersion in the beam do not decrease the fringe visibility considerably. Finally, we briefly present an experiment in preparation to exhibit this localization.

PACS number(s): 07.60.Ly, 39.10.+j, 42.79.Dj

I. INTRODUCTION

Self-imaging of gratings has been investigated extensively in light optics, with well-known examples being the Talbot [1] and Lau [2] effects. In the former case, a grating with period d is illuminated by monochromatic and parallel light (wavelength λ) to create an interference pattern similar to the original grating at distances that are multiples of the Talbot length $L_T=d^2/\lambda$ behind the grating. In the latter example, a grating illuminated by spatially incoherent light is imaged by a second identical grating when the gratings are separated by half the Talbot length and the observation plane is at infinity. Both effects can be explained by classical diffraction and coherence theory [3]. Closely related phenomena with partially coherent light are discussed by Liu [4]. A comprehensive review of the theory and application of self-imaging in optics has been written by Patorski [5]. In addition, self-imaging phenomena have been considered in the context of matter waves in a series of papers by Cowley and Moodie [6].

Recently, these effects have been further investigated and applied to atom optics with de Broglie wavelengths in the 0.1–1-Å range [7]. For example, with a cold beam of potassium atoms Clauser and Li demonstrated an atom interferometer based on a two-grating setup operated in the near field [8] and Ekstrom *et al.* observed first- and higher-order Talbot images behind a single grating with a beam of sodium atoms [9]. However, although certain near-field diffractive imaging techniques have been discussed, it seems not to be generally appreciated that, in theory, a two-grating arrangement allows *localization* of atoms with 100% contrast even with an *extended source* at a *finite* distance. The benefits of imaging with the spatially incoherent illumination of an extended source are twofold: a large atomic flux and the option of mechanically isolating the potentially noisy source from any sensitive experiment downstream. In realizable experiments with a finite source velocity spread and a finite grating extent, contrast of over 90% is achievable on submicrometer scales. This possibility could be of broad importance, including improving experiments in cavity QED that probe the energy spectrum and dynamics of coupled atom-cavity systems [10] and attempts to create arbitrary quantum states of the electromagnetic field [11]. Potential applications may also be found in the field of atom lithography [12].

The purpose of this paper is to extend existing theoretical work by deriving analytical expressions for two-grating near-field imaging from the Fresnel-Kirchhoff diffraction integral. We find an analytical solution for a coherent source (point source). Patterns obtained from sources of finite transverse coherence and especially from infinitely extended sources can then be directly derived by incoherent summation of the point source patterns. We give an intuitive picture of the effect for the simplest case of a large source at infinity. Also, we investigate the importance of inevitably detrimental effects which arise in a real-world experiment via numerical simulation. The paper is organized as follows. In Sec. II we formulate the problem and describe the suggested experimental setup. The theoretical framework underlying the effect is outlined in Sec. III and this work is then used in Sec. IV to calculate patterns resulting from diffractive imaging and the corresponding visibilities behind two gratings. Results of numerical simulations are presented in Sec. V to assess the effects of finite grating width and of nonzero width in the velocity distribution on the ideal-case results. Finally, in Sec. VI we summarize our results and describe possible avenues for implementation.

II. OUTLINE OF THE PROBLEM

For many applications in optics or atomic physics it is important to localize atoms on scales smaller than 1 μm

*Permanent address: Holtronics Technologies, Champs-Montants 12b, CH-2074 Marin, Switzerland. Tel: +41-38-33-68-00.
†Tel: (818) 395-8343; FAX: (818) 793-9506; electronic address: quat@cco.caltech.edu.

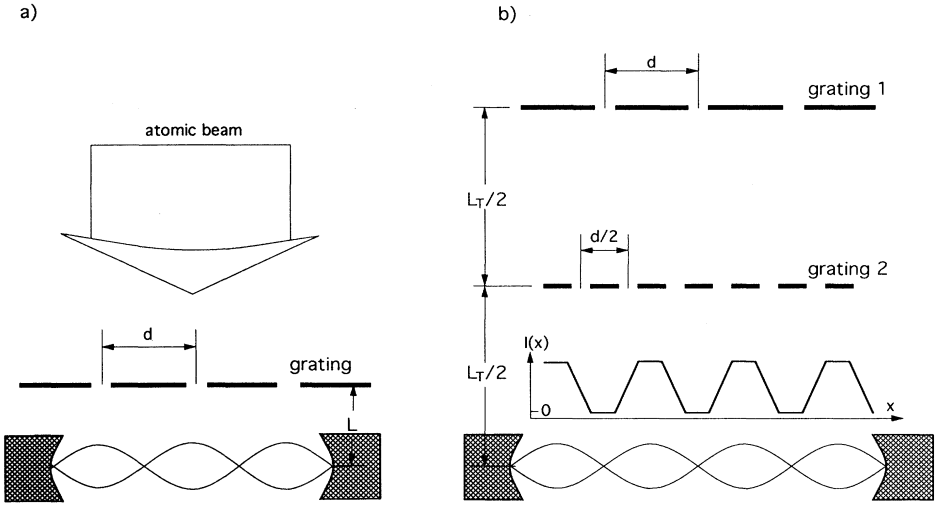

FIG. 1. Two possible setups to localize atoms from a source at infinity to the antinodes of a standing light field. (a) Straightforward approach with one grating very close to the cavity ($L \ll d^2/\lambda_{dB}$) and (b) setup including two gratings separated by half the Talbot length $L_T/2 = d^2/2\lambda_{dB}$. The inset shows the theoretical atomic intensity distribution in the plane of the cavity mode.

as, for example, in cavity QED where it is desirable to confine atoms to the antinodes of an optical standing wave. The straightforward solution is to pass atoms through one grating with a period $d \leq 1$ μm close to the plane of localization [see Fig. 1(a)]. The problems with this setup are that diffraction from the grating leads to a fast washing out of the originally perfect contrast pattern [13] and the need for a very small beam divergence and consequently a small source aperture leads to a drastically reduced atomic flux. As we shall show, these drawbacks can be eliminated by moving the first grating back and introducing a second grating with grating period $d/2$ for an infinite source-grating distance [Fig. 1(b)]. For a specific grating separation, this arrangement produces an interference pattern with period d and with 100% visibility, even for a large source size. In a realistic experiment with finite source-grating separations the grating periods and separations must be modified slightly [see Eq. (9)].

The general setup that we wish to consider is shown in Fig. 2, where an atomic beam is sent through two gratings G_1 and G_2, with grating periods d_1 and d_2. L_1 denotes the distance between grating 1 and 2, L_2 is the distance from grating 2 to the observation plane D, and L_0 is the distance from the source to the first grating. All gratings are assumed to be parallel to each other, to be of zero thickness, and to extend infinitely [14] perpendicular to the plane of Fig. 2, so that the problem can be reduced to two dimensions.

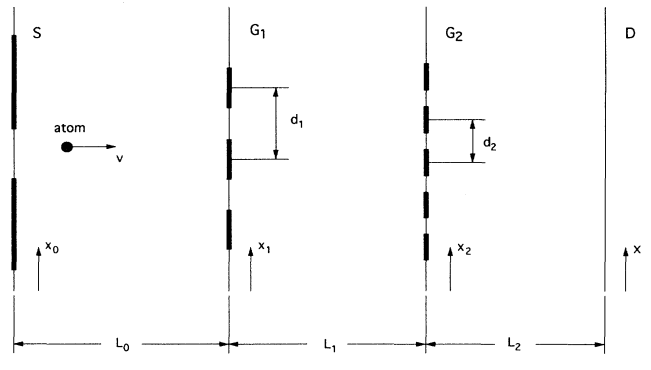

FIG. 2. General two-grating setup. S, source; G_1, first grating with period d_1; G_2, second grating with period d_2; D, detector plane. The corresponding distances between the parallel planes are L_0, L_1, and L_2. The coordinate of a point in one of these planes is given by x_0, x_1, x_2, and x, correspondingly.

The atomic wavelength λ_{dB} depends on the atomic velocity v and mass m: $\lambda_{dB} = h/mv$, where h is Planck's constant. In all subsequent analytical calculations (but not for our numerical results), the gratings are assumed to have an infinite number of slits and the velocity distribution in the beam is taken to be a δ function centered at v. In order to investigate the effects of finite gratings and of nonzero dispersion of atomic velocities in the beam, numerical simulations have been carried out.

III. THEORETICAL FRAMEWORK

Due to the wave character of the atomic center-of-mass motion, the problem of atomic diffraction can be formulated completely analogously to classical diffraction problems in light optics. More precisely, the time-independent Schrödinger equation for one nonrelativistic particle has the form of a Helmholtz wave equation [15] and if internal degrees of freedom of the particles are not of importance, atomic diffraction from small objects can be described by Kirchhoff's scalar theory of diffraction [16]. On the other hand, all effects described below for atoms can also be readily applied to physical optics and indeed to waves in general.

With this preamble and with reference to Fig. 2, let us begin by calculating the probability distribution $I_2(x_2, L_1)$ of finding an atom at transverse position x_2 in the plane of the second grating G_2. We treat the source as an ensemble of incoherent and monochromatic point sources [17] of equal intensity, with the partial amplitude $d\Phi_1^-(x_0, x_1, L_0)$ just to the left of G_1 due to a point

source at position x_0 given by $d\Phi_1^-(x_0,x_1,L_0) \propto e^{ik\sqrt{L_0^2+(x_1-x_0)^2}}$. Here x_1 is the coordinate of a point in the plane of the first grating and $k=2\pi/\lambda_{dB}$ is the absolute value of the atomic wave vector. We introduce the complex amplitude transmission function $t_i(x_i)$, $i=1,2$, which connects the amplitude $d\Phi_i^-(x_i)$ immediately to the left of (before) the grating G_i and the amplitude $d\Phi_i^+(x_i)$ just to the right of (after) the same grating:

$$d\Phi_i^+(x_i)=d\Phi_i^-(x_i)t_i(x_i) . \tag{1}$$

For the gratings used below, the transmission function is real and takes the values 1 (open slit) and 0 (solid bar). The partial amplitude $d\Phi_2^-$ in the plane of the second grating G_2 is calculated by using the Fresnel-Kirchhoff diffraction integral (see, e.g., Ref. [16]) for distances large compared to the grating periods and by making the paraxial approximation

$$d\Phi_2^-(x_0,x_2,L_1) \propto \int_{x_1} d\Phi_1^+(x_0,x_1,L_0) \times \exp[ik\sqrt{L_1^2+(x_2-x_1)^2}]dx_1 . \tag{2}$$

The total intensity distribution at G_1 and subsequent observation planes is found from an incoherent sum over all source point contributions of the form $I_i(x_i) \propto \int_{x_0} |d\Phi_i^-(x_i)|^2 dx_0$. Hence the total intensity distribution just to the left of the second grating G_2 is given by

$$I_2(x_2,L_1) \propto \int_{x_0} |d\Phi_2^-(x_0,x_2,L_1)|^2 dx_0 , \tag{3a}$$

with the point source amplitude

$$d\Phi_2^-(x_0,x_2,L_1) \propto \int_{x_1} t_1(x_1)\exp[ik\sqrt{L_0^2+(x_1-x_0)^2}] \times \exp[ik\sqrt{L_1^2+(x_2-x_1)^2}dx_1 . \tag{3b}$$

Since we are interested in effects occurring in the near field, we retain all terms up to second order in x_i/L_j, $i,j=0,1,2$, in the diffraction integral [18]. In addition, we assume that both gratings are infinitely wide [14] and can therefore develop the transmission function of G_1 as a Fourier series

$$t_1(x_1)=\sum_{n=-\infty}^{\infty} A_n \exp\left[i2\pi n\frac{x_1}{d_1}\right] , \tag{4}$$

with A_n the nth Fourier coefficient. Throughout this paper we will limit our discussion to gratings with infinitely sharp slit edges and a real transmission function. The corresponding model transmission function and its Fourier components are shown in Fig. 3 for a grating with open fraction $f_1=\frac{3}{8}$. With the approximation $\sqrt{L_0^2+(x_1-x_0)^2} \cong L_0+(1/2L_0)(x_1^2+x_0^2-2x_1x_0)$ [and accordingly for the exponent in the third term in Eq. (36)]

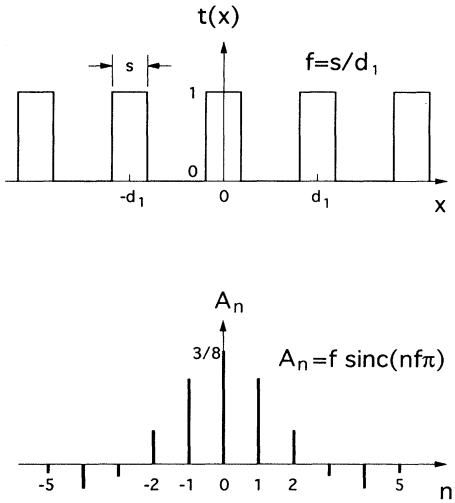

FIG. 3. Transmission function $t(x)$ for an idealized grating with infinitely sharp edges and open fraction $f=\frac{3}{8}$. The corresponding Fourier components $A_n=f\,\mathrm{sinc}(nf\pi)$ up to $n=\pm 5$ are shown below.

we obtain the following equation for the amplitude distribution at G_2 arising from a point source at position x_0 (unimportant phase factors have been removed):

$$d\Phi_2^-(\alpha,\tilde{x}_2,\tilde{L}_1)=C_1\sum_{n=-\infty}^{\infty} A_n \exp[-i\pi\tilde{L}_1(\alpha+n)^2] \times \exp[i2\pi\tilde{x}_2(\alpha+n)] \tag{5}$$

with the dimensionless variables

$$\tilde{L}_1=L_1\frac{\lambda_{dB}}{d_1^2}(1+L_1/L_0)^{-1} , \tag{6a}$$

$$\tilde{x}_2=\frac{x_2}{d_1}(1+L_1/L_0)^{-1} , \tag{6b}$$

$$\alpha=-\frac{d_1}{\lambda_{dB}}\frac{x_0}{L_0} , \tag{6c}$$

and the proportionality factor $C_1=\sqrt{dI_0}(1+L_1/L)^{-1}$, where dI_0 is the beam intensity of the point source right before the first grating. Note that for large source-grating distances, $\tilde{L}_1$ is the grating separation in units of the Talbot length and $\tilde{x}_2$ is the coordinate in units of the grating period d_1. α is defined as the angle under which the point source is viewed from the first grating in units of the far-field first-order diffraction angle λ_{dB}/d_1. The source will be spatially coherent across d_1 if the source aperture extends to a maximum $\alpha_{max} \ll 1$ and incoherent if $\alpha_{max} \gg 1$.

The advantage of developing the transmission function in terms of Fourier components is obvious: in this case the intensity distribution is given simply by a sum and can be easily analyzed for special distances such as, e.g.,

$\tilde{L}_1=1$. If one is not interested in small-scale features (i.e., high diffraction orders) one could truncate the Fourier expansion and limit the discussion to the first few diffraction orders. Here we retain all orders.

The diffraction pattern in the detector plane D arising from the two gratings G_1 and G_2 is calculated in two steps: first, the amplitude $d\Phi_2^+(x_0,x_2,L_1)$ just to the right of the second grating is calculated via Eqs. (1) and (5), where the second grating transmission function is given by

$$t_2(x_2)=\sum_{m=-\infty}^{\infty} B_m \exp\left[i2\pi m\frac{x_2}{d_2}\right] . \tag{7}$$

Second, this amplitude $d\Phi_2^+(x_0,x_2,L_1)$ is combined with the Fresnel-Kirchhoff diffraction integral [see Eq. (2)] for propagation to the detection plane D. The calculation is carried out analogously to the one-grating case. The algebra, however, is tedious and only the final result is given here for the partial amplitude $d\Phi_D(x)$ in the plane D due to a point source at position x_0:

$$\begin{aligned} d\Phi_0(\alpha,\tilde{x},\tilde{L}_1,\tilde{L}_2,p) &= C_2 \sum_{n=-\infty}^{\infty}\sum_{m=-\infty}^{\infty} A_n B_m \exp[-i\pi\tilde{L}_1(\alpha+n)^2] \\ &\quad\times\exp[-i\pi\tilde{L}_2(\alpha+n+pm)^2] \\ &\quad\times\exp[(i2\pi\tilde{x}(\alpha+n+pm)] , \end{aligned} \tag{8}$$

where x is the coordinate in the observation plane (see Fig. 2), $C_2=\sqrt{dI_0}[1+(L_1+L_2)/L_0]^{-1}$, and the dimensionless variables are defined as

$$\tilde{L}_2=L_2\frac{\lambda_{\mathrm{dB}}}{d_1^2}\left[1+\frac{L_1}{L_0}\right]^{-1}\left[1+\frac{L_1+L_2}{L_0}\right]^{-1} , \tag{9a}$$

$$\tilde{x}=\frac{x}{d_1}\left[1+\frac{L_1+L_2}{L_0}\right]^{-1} , \tag{9b}$$

$$p=\frac{d_1}{d_2}\left[1+\frac{L_1}{L_0}\right] . \tag{9c}$$

These expressions are greatly simplified for an infinite source distance $L_0/L_i\to\infty$. In this case, p is simply the ratio of the two grating periods and $\tilde{L}_{1,2}$ are the distances $L_{1,2}$ given in units of the first grating Talbot length. Note that Eq. (8) was found in Ref. [19] for the special case of $L_0\to\infty$. The purpose of this paper is to show that for $p=2$ and $\tilde{L}_1=\tilde{L}_2=\frac{1}{2}$ the atoms can be localized with 100% contrast, even for $L_0/L_i\neq\infty$.

The intensity distribution in the plane D due to an extended source is finally given by

$$I_{\mathrm{ext}}(\tilde{x},\tilde{L}_1,\tilde{L}_2,p)\propto\int_\alpha |d\Phi_D(\alpha,\tilde{x},\tilde{L}_1,\tilde{L}_2,p)|^2 d\alpha . \tag{10}$$

Equations (4)–(10) provide the basis upon which we will now derive a specific two-grating configuration to localize atoms in space.

IV. PATTERNS AND THEIR VISIBILITIES BEHIND TWO GRATINGS

Before discussing patterns associated with two gratings, let us first point out two special cases for the one-grating setup. The starting point for this analysis is Eq. (5), from which we compute multiple images of a point source at $x_0=0$ ($\alpha=0$). At odd multiples of the Talbot distance $\tilde{L}_1=2k-1$, $k\in\mathbb{N}$, the exponential with the quadratic term in Eq. (5) can only take two values: 1 for n even and -1 for n odd. Thus all even terms in the sum are unchanged, whereas odd terms change sign. This corresponds to a downstream image of the original grating shifted by half a period and magnified by a factor $(1+L_1/L_0)^{-1}$. On the other hand, the grating image is unshifted at even multiplies of the Talbot length. This self-imaging phenomenon is called the Talbot effect and was first observed more than 150 years ago. This effect has been used to localize atoms at the Talbot distance behind one grating [9], but in order to attain high contrast, a point source is required since the images are shifted proportionally to α.

Another interesting amplitude distribution is obtained for $\tilde{L}_1=\frac{1}{2}$ and a perfectly rectangular transmission grating with an open fraction $f_1=50\%$, again with $\alpha=0$ for a point source. The Fourier coefficients for this grating are $A_n=\frac{1}{2}\mathrm{sinc}(\pi n/2)$. Since coefficients with even $n>0$ vanish for this grating, the quadratic term in the exponential in Eq. (5) is either 1 for $n=0$ or $-i$ for n odd [which is proved via $n^2=4k(k-1)+1$, $k\in\mathbb{N}$, for n odd]. The resulting probability amplitude is therefore given by $d\Phi_2^-(\tilde{x}_2)\propto\frac{1}{2}(1+i)-it(\tilde{x}_2)$, a function that takes only the two values $(1/\sqrt{2})e^{\pm i\pi/4}$. The intensity is constant, whereas the phase jumps between $\pi/4$ and $-\pi/4$ over one grating period. This somewhat amazing field distribution may be useful in connection with phase-sensitive techniques in atom interferometry.

These examples show that in the near field, gratings can behave in "unfamiliar" ways and that the characteristic distances for self-imaging are given by $L_T\approx d^2/\lambda_{\mathrm{dB}}$ ($\tilde{L}_1\approx 1$). These simple observations drive the search for similar effects with two gratings. In particular, Chang, Alferness, and Leith [19] observed that under special conditions two gratings with periods $d_1=2d_2$ can self-image without requiring either a point source (in contrast to the one-grating examples given above) or a monochromatic beam. Additionally, Clauser and Li [8] have used this grating configuration for atom interferometry, but a quantitative analysis of high-contrast localization with an incoherent source was not given. For this specific two-grating setup we now derive a simple analytical expression for the case of perfectly rectangular transmission functions.

In Eq. (9a) we choose $p=2$, (which is the generalization of the condition $d_1=2d_2$ for infinite source-grating distances) and $\tilde{L}_1=\tilde{L}_2=\frac{1}{2}$ and rewrite Eq. (8) as follows by omitting unimportant phase factors and by regrouping terms:

$$d\Phi_D(\alpha,\tilde{x},\tilde{L}_1=\tilde{L}_2=\tfrac{1}{2},p=2)\equiv d\Phi_D(\alpha,\tilde{x})=C_2\sum_n\sum_m A_nB_m\exp\left[-i\frac{\pi}{2}\{n^2+(n+2m)^2\}\right]\times\exp[-i2\pi(n+m)\alpha]\exp[i2\pi(n+2m)\tilde{x}]\ . \tag{11}$$

This expression can be readily simplified by using the following identity

$$\exp\left[-i\frac{\pi}{2}\{n^2+(n+2m)^2\}\right]=\begin{cases}1 \text{ for } n \text{ even}\\ -1 \text{ for } n \text{ odd}\ ,\end{cases} \tag{12}$$

independent of m. As a result, the two summations over n and m can be factorized:

$$d\Phi_D(\alpha,\tilde{x})\propto\left\{\sum_n A_n\exp[i2\pi n(\tilde{x}-\alpha)]\exp[-i\pi n]\right\}\times\left\{\sum_m B_m\exp[i2\pi m(2\tilde{x}-\alpha)]\right\}\ . \tag{13}$$

This can now be written in terms of the transmission functions t_1 and t_2 of the first and second gratings [as given in Eqs. (4) and (7)]:

$$d\Phi_D(\alpha,\tilde{x})=C_2t_1[(\tilde{x}-\alpha-\tfrac{1}{2})d_1]t_2[(2\tilde{x}-\alpha)d_2]\ . \tag{14a}$$

The final probability amplitude arising from a point source at the origin ($\alpha=0$) is therefore simply given by the product of the transmission function of the first grating, shifted by half a period, and the transmission function of the second grating. Equation (14a) is the central result of this paper. It describes how the intensity pattern in the detector plane can be obtained when illuminating the two-grating setup coherently with a point source. Any partially coherent source distribution and its pattern can be derived from this equation.

With the point source at infinity, Eq. (14a) can be readily expressed in real-space coordinate x because in this special case $d_1/d_2=2$, $x=\tilde{x}d_1$, and hence

$$I_D(x,\alpha=0)=dI_0t_1(x-d_1/2)t_2(x)\ . \tag{14b}$$

The corresponding intensity distributions for the two cases of perfectly rectangular gratings and open fractions $f_1=25\%$ and 50% for the first grating and $f_2=50\%$ for the second grating are shown in Figs. 4(a) and 4(b). The point source patterns for $f_1=25\%$ and 50% are identical and consist of a perfectly rectangular pattern with open fraction 25%, which is shifted with respect to the origin by $d_1/2$. Note that the intensity maxima are given by dI_0, although the total overall transmission of the two gratings is different in the two cases. For sources at finite distances, the result is the same with the exception that the period is $d_1[1+(L_1+L_2)/L_0]$ and the intensity is reduced by a factor $[1+(L_1+L_2)/L_0]^{-2}$.

Given the result of Eq. (14a) for a point source the principal question remaining is, What happens if we take an extended source for which α runs from $-\alpha_{\max}$ to $+\alpha_{\max}$? Does the fringe visibility persist or is it washed out completely as soon as $\alpha_{\max}\gg1$ [20], as is the case for a diverging beam from an extended source? This question is answered by applying Eq. (10) to Eq. (14a) and using the identity $|t_{1,2}(\tilde{x})|^2=t_{1,2}(\tilde{x})$ for perfectly rectangular transmission gratings to find that

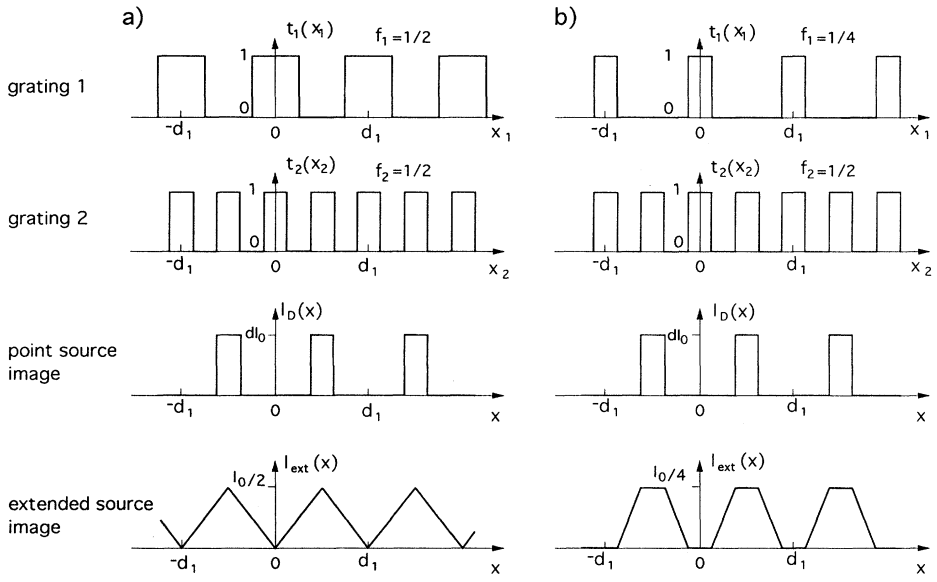

FIG. 4. Self-images behind two gratings for a point source and for an extended source, both with $L_0\to\infty$. The distances are $L_1=L_2=L_T/2$ and open fraction of second grating is $f_2=50\%$. The transmission functions of the two gratings $t_i(x_i)$ and the resulting intensity distributions for a point source at $x_0=0$ (I_D) and an extended source (I_{ext}) are shown for an open fraction of grating 1 (a) $f_1=50\%$ and (b) $f_1=25\%$.

$$I_{\text{ext}}(\tilde{x},\tilde{L}_1=\tilde{L}_2=\tfrac{1}{2},p=2)\equiv I_{\text{ext}}(\tilde{x})\propto\frac{1}{2\alpha_{\max}}\int_{-\alpha_{\max}}^{\alpha_{\max}}t_1[(\tilde{x}-\alpha-\tfrac{1}{2})d_1]t_2[(2\tilde{x}-\alpha)d_2]d\alpha$$
$$=\frac{1}{2\alpha_{\max}}\int_{-\alpha_{\max}}^{\alpha_{\max}}t_1[(\alpha+\tilde{x}+\tfrac{1}{2})d_1]t_2(\alpha d_2)d\alpha\ , \tag{15}$$

which looks like a convolution of grating 2 with the shifted grating 1. The factor $\frac{1}{2}\alpha_{\max}$ was added to ensure convergence of the integral for $\alpha_{\max}\to\infty$. If the source dimension is much larger than $L_0\lambda_{\text{dB}}/d$, then $\alpha_{\max}\gg 1$ and the integral is to a good approximation independent of the upper and lower limits and $\alpha_{\max}$ can be set to infinity. Due to the periodicity of the expression under the integral, it is therefore sufficient to evaluate the integral within one period $0<\alpha<1$. For two rectangular gratings (G_1,G_2) with open fractions (f_1,f_2) $(f_i\le 0.5)$, respectively, the result is $[f_{\min}:=\min(f_1,f_2)]$

$$I_{\text{ext}}(\tilde{x})=\begin{cases}0 \quad \text{for } n-\dfrac{1-f_1-f_2}{2}\le\tilde{x}\le n+\dfrac{1-f_1-f_2}{2}\\ I_0 f_{\min} \quad \text{for } n+\dfrac{1-|f_1-f_2|}{2}\\ \qquad\qquad\le\tilde{x}\le n+\dfrac{1+|f_1-f_2|}{2}\ ,\end{cases} \tag{16}$$

where n is an integer and $I_{\text{ext}}(\tilde{x})$ is linearly increasing or decreasing in between. I_0 is the total beam intensity to the left of grating 1.

For illustration of this final result, we take again the above examples of $f_1=25\%$ and 50% and $f_2=50\%$ for the two gratings. The intensity distributions $I_{\text{ext}}(x)$ for illumination by an infinitely extended source are shown in Figs. 4(a) and 4(b) at the bottom. Although the point-source images are identical, the large-source images differ considerably. For $f_1=50\%$ [Fig. 4(a)] the resulting image is a perfect triangular sawtooth with a maximum intensity equal to half the incoming intensity. The main problem with this setup is the fact that the intensity drops to zero only at the singular points $\tilde{x}=n$, where n is an integer. This situation is clearly not ideal for an experiment with usually finite position resolution.

By contrast, for $f_1=25\%$ [Fig. 4(b)] the intensity drops to zero not only at singular observation points but for all $\tilde{x}$ in the intervals $n-\frac{1}{8}\le\tilde{x}\le n+\frac{1}{8}$, $n\in\mathbb{Z}$, and the contrast is therefore 100% even with a nonideal detector. The price to be paid for this improved localization is that the maximum intensity drops to $I_0/4$. However, this case offers a reasonable compromise between high atomic flux and good localization.

The origin of this unexpected result of high contrast even for an extended source is somewhat obscured by the lengthy equations. To conclude this section, we will give two somewhat more intuitive pictures of the effect for the simplest case of a large extended source located far from the gratings ($\alpha_{\max}\gg 1$ and $L_0/L_{1,2}\gg 1$). The first explanation of the effect is found by considering G_1 itself as the (structured) source and reducing the problem to imaging with a single grating G_2. The pattern due to a point source in the plane of G_1 is given by Eq. (5) and by replacing L_0 by L_1, L_1 by L_2, and d_1 by d_2 in Eq. (6). As a consequence, $\tilde{L}_1=1$ and we end up with the simple Talbot effect described at the beginning of Sec. IV. The resulting pattern I_2^-, however, has a period of d_1 (and not d_2) due to the factor $(1+L_2/L_1)^{-1}$ in Eq. (6b). This point-source image must now be convolved with the transmission function of G_1 to obtain the final intensity distribution. Since both t_1 and I_2^- have the same period d_1, the self-imaging pattern survives. In this picture we also see that analogous to the Talbot effect, localization with period d_1 occurs not only for one specific distance, but for all distances $L_1=L_2=nL_T/2$, $n\in\mathbb{N}$.

Our second explanation is based on the complex coherence function μ_{12}, as defined in [16]. This approach has already been used by other authors to explain the Lau effect [21]. The coherence function is the time-averaged product of the field amplitude at position x with the amplitude at position $x+\Delta x$ and indicates the degree of spatial coherence for the amplitude from an extended source. If one knows the intensity distribution of an incoherent source in the plane σ, then μ_{12} in a plane parallel to σ at distance L is given by

$$\mu_{12}(q)=e^{i\psi}\frac{\int_\sigma I(\xi)e^{-ikq\xi}d\xi}{\int_\sigma I(\xi)d\xi}\ ,$$
$$\psi=\frac{k}{2L}[(x+\Delta x)^2-x^2]\ , \tag{17}$$

where q is defined as $\Delta x/L$ and ξ is the transverse position in the source plane σ. Let us now just consider the simplest case of a large extended source located far from the gratings corresponding to a completely incoherent irradiation of grating 1. In this case, grating 1 (with period d_1 and N slits) can itself be considered as an incoherent source. For a first grating G_1 with 50% open fraction, we find from Eq. (17) that μ_{12} takes the following form in the plane of the second grating G_2:

$$\mu_{12}(q_2)\propto\operatorname{sinc}\left[\frac{kq_2d_1}{4}\right]\frac{\operatorname{sinc}\left[N\dfrac{kq_2d_1}{2}\right]}{\operatorname{sinc}\left[\dfrac{kq_2d_1}{2}\right]}\ ,$$
$$q_2\equiv\Delta x_2/L_1\ . \tag{18}$$

For $N\to\infty$ the second term in Eq. (18) can be approximated by a sum of Dirac δ functions: $\sum_n(-1)^n\delta(kq_2d_1-n2\pi)$. Hence, for $L_1=L_T/2$

$=(d_1)^2/2\lambda_{dB}$ any two points x_2' and x_2'' in this plane are highly correlated if they are separated by a multiple of $d_1/2$. By introducing now a grating with period $d_2=d_1/2$ into this plane, only correlated points (oscillating perfectly in phase or out of phase) are transmitted. Grating G_2 thus acts as a secondary phased source, which produces a simple interference pattern in a plane $L_T/2$ behind this second grating, as can be seen from the following formula relating the coherence function in the plane of the second grating to the intensity in the observation plane D (located $L_T/2$ away from G_2) [22]:

$$I(x)\propto\int_{x_2'}dx_2'\int_{x_2''}dx_2''\mu_{12}\left[\frac{x_2''-x_2'}{L_T/2}\right]t_2(x_2'')t_2(x_2') \times\exp[ik(s''-s')]\ , \tag{19}$$

with s' and s'' the distances from a point x in the observation plane to points x_2' and x_2'' in the plane G_2, respectively. In the Fresnel approximation this integral can be readily evaluated by inserting the coherence function from Eq. (18) and by assuming a second grating with infinitely narrow slits ($f_2\to 0$). In this case the coordinates in the grating 2 can be replaced by $x_2'=md_1/2$ and $x_2''=(m+n)d_1/2$, where m and n are integers; each integral is then transformed into a sum over n or m. With $t_2(x_2'+nd_1/2)t_2(x_2')=t_2(x_2')$, $n\in\mathbb{Z}$, and $k(s''-s')\cong-(2\pi/d_1)nx+\psi$, $\psi=n^2(\pi/2)+\pi mn$, $I(x)$ takes the form

$$I(x)\propto\sum_n \operatorname{sinc}\left[n\frac{\pi}{2}\right]\exp\left[in\frac{2\pi}{d_1}x\right] \times\exp(in^2\pi)=t_1\left[x-\frac{d_1}{2}\right]\ , \tag{20}$$

which is simply the transmission function of the first grating shifted by half a period. This result also follows directly from Eq. (16) with $f_1=\frac{1}{2}$ and $f_2\to 0$.

We can now give an intuitive picture of the effect as follows. A periodic incoherent source (grating 1) with period d_1 produces strong correlations between points separated by $d_1/2$ in a plane $L=L_T/2$ away from the source G_1. By transmitting with G_2 only those parts of the wave function that have a high correlation in this plane, we obtain a pattern with high contrast in a subsequent plane, located at $L=L_T$ away from the source grating G_1.

V. NUMERICAL SIMULATIONS FOR A REALISTIC EXPERIMENTAL SETUP

All of our preceding analytical calculations were carried out under the idealized assumptions of infinite gratings (along x_i) and monochromatic illumination. If instead the gratings are finite, then from the coherence-function picture just presented one might expect that the error would be small as long as the first grating consists of more than $N_1\approx 10$ slits. To verify this statement, we have performed a rigorous numerical calculation of the diffraction pattern with finite grating sizes as well as with finite-width velocity distributions in the atomic beam. The calculations are performed using an algorithm described in Ref. [23] which minimizes computer time by converting the diffraction integrals into convolutions, thereby exploiting fast Fourier transform techniques in the computations. The calculations were performed on a Macintosh Quadra 700 whose memory is sufficient for storing the large vectors used in these calculations.

For the numerical simulations, we used two sets of parameters, listed in Table I. The first set of parameters (set I) forms a numerical "test" set which satisfies Eqs. (9) with a localization period of 426 nm (equal to the optical standing wave period $\lambda_{light}/2$ in our cavity QED experiments [8]). The second set of parameters (set II) for the gratings and the source was chosen according to an experiment planned with a seeded supersonic beam of cesium in combination with microfabricated silicon nitride gratings [24]. Note that, due to the finite source distance, the period of the first grating is not exactly twice the period of the second one and is smaller than the period of 426 nm obtained in the detector plane. Limited computer memory keeps the source size in our calculations at only 10 μm for point resolution of 1 nm. This source size corresponds to $\alpha_{max}\approx 1$, which obviously does not meet the requirement of $\alpha_{max}\gg 1$, but is sufficient to smear out the point source image over one grating period. In the planned experiment we will use a source about 0.5 mm in diameter to obtain a gratinglike intensity pattern in the atomic beam allowing localization of atoms to the antinodes of a standing-wave field in an optical cavity.

In a first numerical evaluation run (using numerical value set I) we confirmed that the image visibility, with $f_1=25\%$, remains high even for finite-sized gratings. We determined the visibility V by measuring the average maximum and minimum intensity values I_{max} and I_{min} near the center of the calculated fringe pattern and by using the definition

TABLE I. The two sets of parameter values used for the numerical calculations. Set I is the test set and is used for Fig. 5. Set II is based on values for a proposed experiment and is used in Figs. 6 and 7.

Parameter	Numerical value I	Numerical value II
λ_{dB} (m)	3.7×10^{-12}	3.7×10^{-12}
L_0 (m)	0.65	0.65
L_1 (mm)	22.13	21.9
L_2 (mm)	23.69	23.4
d_1 (nm)	398	396
d_2 (nm)	206	204
Localization period (nm)	426	426

$$V=\frac{I_{\max}-I_{\min}}{I_{\max}+I_{\min}} . \tag{21}$$

By going from $N_1=N_2/2=20$ (same widths for the two gratings) down to $N_1=5$ we have found that the visibility remains roughly constant (this is confirmed in Fig. 7). For example, the intensity distribution for $N_1=20$ is shown in Fig. 5 as a function of transverse position x in the detector plane, where we note that due to the finite grating size, no sharp corners appear as in the theory. For a comparison with Fig. 4, we have plotted the results of numerical simulations for $f_1=50\%$ and $f_2=50\%$ in Fig. 5(a) [compare Fig. 4(a)] and for $f_1=25\%$ and $f_2=50\%$ in Fig. 5(b) [compare Fig. 4(b)]. In Fig. 5(a), the expected angular minima are smeared out due to the diffraction from the grating edges and, as a consequence, the visibility drops to about 86%. By contrast, in Fig. 5(b) with $f_1=25\%$, the intensity stays low for about a quarter of a period as in the analytical result. The minima do not, however, go all the way to zero, but still the contrast remains high at 97%. The advantage of using a first grating with lower open fraction is evident.

Due to the fact that the two-grating localization depends on the wavelength of the particles through Eq. (9a), a velocity spread in the beam will deteriorate the effect. The role of *nonzero velocity dispersion* is investigated by

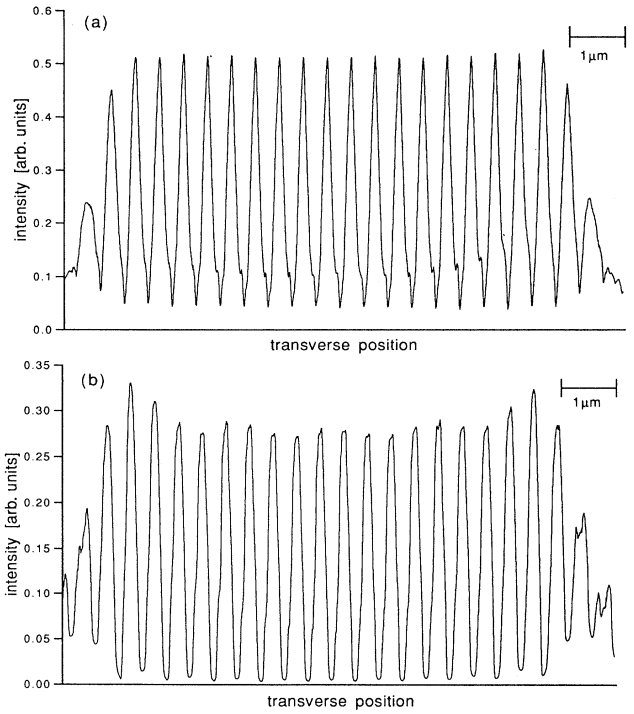

FIG. 5. Results of the numerical simulations (numerical values set I) for $N_1=N_2/2\approx 20$ and a monochromatic source. Intensity distribution in the detector plane for (a) $f_1=f_2=\frac{1}{2}$ and (b) $f_1=f_2/2=\frac{1}{4}$. The asymmetries are due to an arbitrary cutoff of the gratings on both sides (partial slits at both ends are possible).

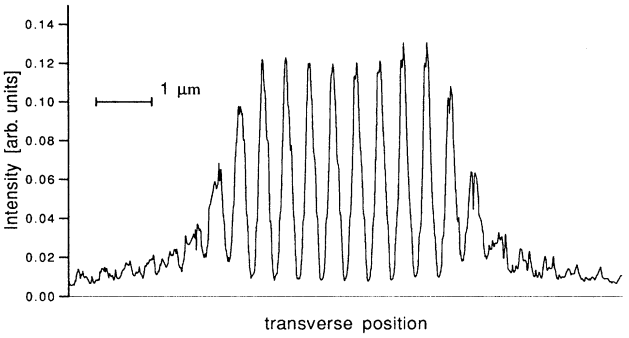

FIG. 6. Numerical result (numerical values II) for a finite width in the velocity distribution such that $\lambda_0/\Delta\lambda=20$. The parameters are from numerical values set II and $f_1=f_2/2=\frac{1}{4}$. The visibility here is 87%.

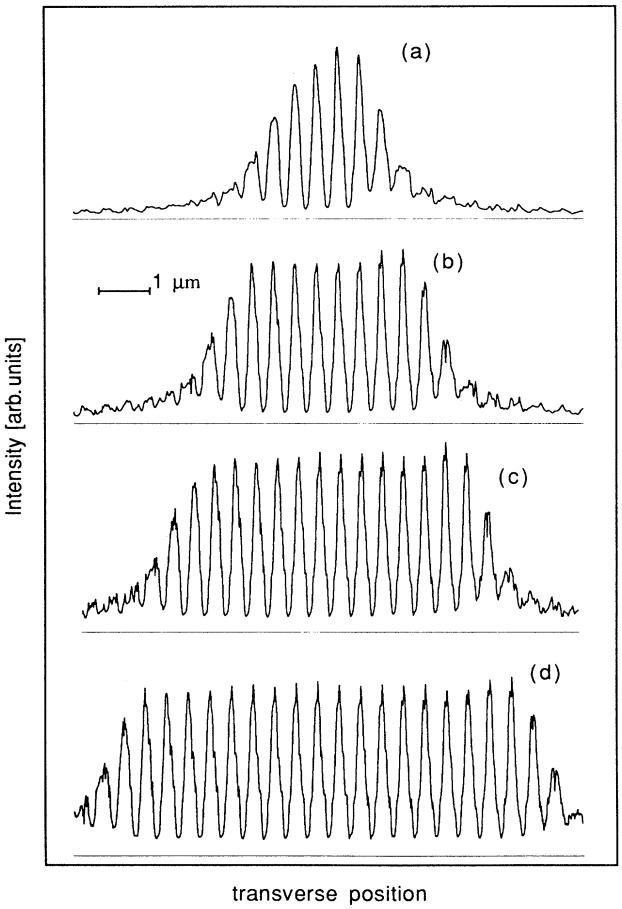

FIG. 7. Same as in Fig. 6, but for a sequence of different grating sizes: (a) $N_1\approx 5$, (b) $N_1\approx 10$, (c) $N_1\approx 15$, and (d) 20. The relative amount of atoms in the unstructured wings decreases with grating size, whereas the visibility stays almost constant. Note that (b) is the same as Fig. 6.

calculating the intensity patterns for different de Broglie wavelengths and weighting each result incoherently by a function $N(\lambda)$ corresponding to a Gaussian velocity profile for the beam [25]:

$$N(\lambda)d\lambda = N_0 \exp\left[-\left[\frac{\lambda-\lambda_0}{\Delta\lambda}\right]^2\right] d\lambda \ .$$

The numerical result for numerical values set II with a finite wavelength width $\lambda_0/\Delta\lambda = 20$ ($\lambda_0 = 3.7\times10^{-12}$ m), as we have measured in our seeded cesium beam, is shown in Fig. 6 for $N_1 \approx 10$ slits. Relative to Fig. 5(b), the visibility drops by about 10% to a value of 87%, but otherwise the patterns are comparable. This demonstrates that a supersonic beam is sufficient to suppress dispersion effects and that less-than-exact grating periods and separations are sufficient for good localization. For completeness, in Fig. 7 we show the self-imaging patterns for the above velocity distribution for various grating sizes. These results are for $N_1 = 5$ up to 20, showing that the visibility at the center of the pattern changes little when the number of slits is changed. The total relative number of atoms in the unstructured wings on both sides of the fringe pattern, however, decreases linearly with grating size. Large gratings are therefore more efficient for localization. In the actual experiment we will use gratings with $N_1 \approx 100$. These two tests clearly show that the localization effect discussed in this paper is relatively robust to deviations from the ideal case and should be clearly observable in a realistic apparatus with high atomic flux.

VI. CONCLUSIONS

We have shown that, even with an extended source, atomic patterns of high contrast with submicrometer resolution can be produced with a simple two-grating setup, where the grating period of grating 2 is approximately half that of grating 1 and the grating separation is approximately half the Talbot length of the first grating. This setup should not only allow significant atomic localization but should also yield high atomic fluxes and high mechanical stability due to grating separations in the centrimeter range. Although we have restricted our analysis to the case of perfect rectangular gratings, the two-grating setup could also yield interesting results for phase gratings created by optical fields. We are currently building an experiment with cesium atoms to observe this interference and to apply the technique to experiments in optical cavity QED.

ACKNOWLEDGMENTS

The research was funded by the Office of Naval Research and by the National Science Foundation. O.C. would like to thank the Schweizerische Nationalfonds for financial support for his research at Caltech.

[1] F. Talbot, Philos. Mag. **9**, 401 (1836).
[2] E. Lau, Ann. Phys. (Leipzig) **6**, 417 (1948).
[3] F. Gori, Opt. Commun. **31**, 4 (1979).
[4] L. Liu, J. Opt. Soc. Am. A **5**, 1709 (1988).
[5] K. Patorski, in *Progress in Optics Volume XXVII,* edited by E. Wolf (Elsevier, Amsterdam, 1989), pp. 1–108.
[6] J. M. Cowley and A. F. Moodie, Proc. Phys. Soc. London Sec. B **70**, 486 (1957); **70**, 497 (1957); **70**, 505 (1957); **76**, 378 (1960).
[7] J. F. Clauser and M. W. Reinsch, Appl. Phys. B **54**, 380 (1992).
[8] J. F. Clauser and S. Li, Phys. Rev. A **49**, R2213 (1994).
[9] Localization of sodium atoms has been observed by using the Talbot effect: C. R. Ekstrom, M. Chapman, T. Hammond, and D. E. Pritchard (private communication).
[10] R. J. Thompson, G. Rempe, and H. J. Kimble, Phys. Rev. Lett. **68**, 1132 (1929).
[11] A. S. Parkins, P. Marte, P. Zoller, and H. J. Kimble, Phys. Rev. Lett. **71**, 3095 (1993).
[12] J. J. McClelland, R. E. Scholten, E. C. Palm, and R. J. Celotta, Science **262**, 877 (1993), and references therein.
[13] Numerical calculations show that the visibility drops to 80% within a distance of $0.1d^2/\lambda_{dB}$ behind the grating.
[14] If taken rigorously, the assumption of an infinite grating is not compatible with the Fresnel approximation as given in connection with Eqs. (1)–(6). Infinity in our case means that the number of slits in a grating $N \gg 1$. For the experimental parameters given in Sec. V, even $N = 1000$ leads to grating dimensions small enough to neglect fourth-order terms in $\Delta x_i/L$, $\Delta x_i = x_i - x_1$, in the expansion of the exponential in Eq. (3b).
[15] V. Sears, *Neutron Optics* (Oxford University Press, New York, 1989).
[16] M. Born and E. Wolf, *Principles of Optics,* 6th ed. (Pergamon, New York, 1989), p. 375.
[17] The two conditions of spatial incoherence and monochromaticity are incompatible if taken rigorously, but they can be justified in most cases. See Ref. [16], Chap. X and especially the footnote on p. 509 for a discussion of this.
[18] This approximation is known as Fresnel approximation; see Ref. [16], Chap. VIII.7, p. 428.
[19] B. J. Chang, R. Alferness, and E. N. Leith, Appl. Opt. **14**, 1592 (1975).
[20] This is possible without violating the paraxial approximation.
[21] R. Sudol and B. J. Thompson, Opt. Commun. **31**, 105 (1979).
[22] See, e.g., Ref. [16], p. 517.
[23] Q. A. Turchette, D. E. Pritchard, and D. W. Keith, J. Opt. Soc. Am. A **9**, 1601 (1992).
[24] The silicon nitride gratings were fabricated at the National Nanofabrication Facility at Cornell University. The fabrication procedure is described in D. W. Keith, R. J. Soave, and M. J. Rooks, J. Vac. Sci. Technol. B **9**, 2846 (1991).
[25] The wavelength distribution is actually given by $N(\lambda)d\lambda = C\lambda^{-7}\exp\{-[(\lambda-\lambda_0)/\Delta\lambda](\lambda_0/\lambda)^2\}d\lambda$, but the error is negligible for $\lambda_0/\Delta\lambda = 20$.